Life Sciences 237 (2019) 116943

Contents lists available at ScienceDirect

Life Sciences

journal homepage: www.elsevier.com/locate/lifescie

Artemisinin attenuates the development of atherosclerotic lesions by the regulation of vascular smooth muscle cell phenotype switching

Hongjiao Du, Qiao Zhao, Hongbin Zang, Cheng Chang, Xiaodong Li*

Department of Cardiology, Shengjing Hospital of China Medical University, Shenyang, 110004, PR China

ARTICLE INFO

Keywords:
Atherosclerosis
Artemisinin
RNA sequencing
VSMC phenotype switching

ABSTRACT

Aims: The purpose of this study was to investigate the therapeutic effect of artemisinin (ART) on atherosclerosis and explore the molecular mechanisms involved by RNA sequencing (RNA-Seq).

Main methods: Eight-week-old male ApoE$^{-/-}$ mice were treated with ART for eight weeks. Atherosclerotic lesion sizes were determined by Oil Red O staining, and RNA-Seq was used to detect the profile of differentially expressed genes following the administration of ART. The expressions of contractile phenotypic markers were detected by western blot and qRT-PCR, and the ability of the MOVAS cells to migrate and proliferate were assessed using the wound healing and CCK8 assays.

Key findings: Artemisinin treatment significantly reduced plaque area in the ApoE$^{-/-}$ mice and increased the expression of contractile phenotypic markers. RNA-Seq of aorta tissue revealed a distinct change in gene expression patterns after the mice were treated with ART. Our bioinformatics analysis demonstrated that the most prominently enriched pathway was a set of genes involved in vascular smooth muscle contractile function. Using an *in vitro* cell model, we demonstrated that ART could effectively reverse PDGF-activated MOVAS migration and proliferation, and elevate the level of proteins involved in the contractile phenotype.

Significance: We provide *in vivo* and *in vitro* evidence supporting a role for ART in the suppression of atherosclerosis, partly through the inhibition of vascular smooth muscle cell phenotype switching to a de-differentiated phenotype. These data further advances our understanding for a potential role for ART and suggests that ART is an excellent candidate for the treatment of atherosclerosis.

1. Introduction

Atherosclerosis is the buildup of plaques containing cholesterol crystals, cell debris, and collagen fibers in the intima of arteries. As the major pathological process underlying coronary artery diseases, cerebral ischemic stroke, and peripheral vascular diseases, atherosclerosis has been the leading cause of death globally [1]. Despite the current advances in drug therapy to reduce hypertension and lower lipids [2], atherosclerosis continues to impose immense health and economic burdens on society. Many cell types are involved in atherosclerosis progression and become dysfunctional during its development and progression [3]. Therefore, it is desirable to find a drug that can target and modulate the processes involved in atherosclerosis.

Recently, studies applying the emerging techniques of lineage-tracing [4–6] and single-cell sequencing [7–9] for unbiased identification and tracking of vascular smooth muscle cells (VSMCs) have demonstrated that 40–70% of the cells in plaques originate from VSMCs. Furthermore, these cells underwent de-differentiation and converted to multiple alternative phenotypes during atherosclerosis progression. These findings demonstrated that VSMC phenotypic switching plays a critical role in atherosclerosis development. The VSMC is a differentiated cell type (called differentiated or contractile phenotype) located in the medial layer of healthy arteries [10]. They rarely proliferate or migrate and express a variety of unique contractile proteins (e.g., αSMA, Calponin1, SM22α, and SMMHC), which are required for their contractile function [11]. However, in atherosclerosis, VSMCs undergo phenotypic switching to a de-differentiated phenotype characterized by a reduction in contractile gene expression and an enhanced migration and proliferation ability [12,13]. The current view is that the inhibition of VSMC phenotypic switching to the de-differentiated phenotype has an atheroprotective role [14,15] and modulating this process could be an efficient therapeutic strategy for an anti-atherosclerosis treatment [16].

Artemisinin (ART), is a sesquiterpene lactone endoperoxide first isolated by Tu Youyou from Artemisia annua L (sweet wormwood) [17]. It is known for its potent anti-malarial effects and reliable safety

* Corresponding author. Department of Cardiology, Shengjing Hospital of China Medical University, 36 Sanhao Street, Shenyang, 110004, PR China.
E-mail address: lixd@sj-hospital.org (X. Li).

https://doi.org/10.1016/j.lfs.2019.116943
Received 20 August 2019; Received in revised form 29 September 2019; Accepted 7 October 2019
Available online 08 October 2019
0024-3205/

record [18]. Interestingly, extensive research in the recent years has found that the activity of ART is not restricted to malaria, but has therapeutic benefits in many other diseases such as cancer [19], systemic lupus erythematosus [20], viral infections [21], obesity [22], and fibrosis [23]. However, little work has been performed on the therapeutic effect of ART on atherosclerosis.

This study aimed to investigate the pharmacological effect of ART on atherosclerosis and its underlying mechanism of action. We selected the ApoE $^{-/-}$ mice (the most widely used experimental animal model of atherosclerosis [24]) to create an animal model of atherosclerosis and then to treat them with ART. To get an overall in-depth picture of the changes that have taken place at the molecular level, we performed RNA-Seq of the mouse aortas. The results of our bioinformatics analysis indicated that the vascular smooth muscle contraction functional set was the most significantly changed pathway, therefore we hypothesized that ART might attenuate the progression of atherosclerosis through the inhibition of VSMC phenotype switching to the de-differentiated phenotype. To test this hypothesis, we conducted both *in vivo* and *in vitro* experiments on the effects of ART against atherosclerosis. Our results showed that ART alleviated atherosclerotic lesions partly by the inhibition of VSMC phenotype switching to the de-differentiated phenotype.

2. Materials and methods

2.1. Animal experiments

All animal experiments were performed in accordance with the National Institutes of Health Guide for the Care and Use of Laboratory Animals (NIH Publications No. 8023, revised 1978) and the European Convention for the Protection of Vertebrate Animals Used for Experimental Purposes (Council of Europe, 1986). The experimental procedures were approved by the Animal Ethics Committee at Shengjing Hospital, China Medical University (2018PS513K).

Male C57BL/6 mice and Apolipoprotein E-deficient (ApoE $^{-/-}$) mice from the same gene background at eight weeks of age were purchased from Beijing Huafukang Biotechnology Co., Ltd. (Beijing, China). The C57BL/6 mice were fed a standard rodent chow diet for eight weeks and served as the control group (CON). The ApoE $^{-/-}$ mice were randomly divided into three groups: Atherosclerosis group (AS) in which mice were given Western Diets (21% fat, 0.15% cholesterol, Beijing Huafukang Biotechnology, NO: H10141) for eight weeks; low-dose treatment group (ART-L) in which mice were administered orally with 50 mg/kg/day ART (purity ≥98%, Beijing Solarbio Life Sciences, IA0520) for eight weeks and fed a Western Diet; and the high-dose treatment group (ART-H) in which mice were administered orally with 100 mg/kg/day ART for eight weeks and fed a Western Diet.

The mice were housed in a room with a 12/12-h dark/light cycle, a humidity of 45–55% and a temperature of 22 ± 1 °C with free access to food pellets and water. All the mice were euthanized with an intraperitoneal injection of pentobarbital at 16 weeks of age. The intact aortas and aortic roots were carefully dissected free of adherent adipose tissue, washed with phosphate buffer saline (PBS), and immediately stored in liquid nitrogen or fixed in 4% paraformaldehyde (4% PFA) for downstream experiments.

2.2. Oil Red O staining

The aortic roots were fixed in 4% PFA for 48 h and then transferred into PBS containing 30% sucrose (w/v) overnight at 4 °C and then embedded in tissue freezing medium (Sakura Tissue-Tek® O.C.T.). The sizes of the atherosclerotic lesions in the aortic roots were determined by Oil Red O (Sigma-Aldrich O-0625) staining, as previously described [25]. Briefly, serial frozen sections (10 μm thick) of the aortic root (from the appearance of the three aortic valves to where the aortic wall disappears) were collected. Five sections separated by 100 μm from each other were stained with Oil Red O. Positively stained areas of the five sections from each animal were quantified using ImageJ software by an investigator blinded to the experimental conditions and the results were presented as a mean lesion area.

2.3. Hematoxylin and eosin staining

The aortic roots were embedded in paraffin and sliced into 4 μm sections.

Then the sections were deparaffinized, rehydrated, and stained with hematoxylin and eosin (H&E), according to a standard protocol from our laboratory. Morphological features of atherosclerotic plaque were observed under a light microscope (Nikon Eclipse NI, Japan).

2.4. RNA-sequencing and gene expression analysis

Total RNA extracted from aorta samples from mice in the AS and ART-L groups was sent to Novogene Genome Sequencing Company (Beijing, China) for RNA-Seq analysis. The RNA integrity was assessed using the RNA Nano 6000 Assay Kit of the Bioanalyzer 2100 system (Agilent). Sequencing libraries were generated using the rRNA-depleted RNA by NEBNext® Ultra™ Directional RNA Library Prep Kit from Illumina® (NEB, USA), following the manufacturer's recommendations. The libraries were sequenced on an Illumina Hiseq 4000 platform, and 150 bp paired-end reads were generated. The raw reads were assessed for quality using FastQC, and mapped to the reference genome using HISAT2 (v2.0.4) [26] and gene expression levels were quantified using Cuffdiff (v2.1.1) [27]. Gene expression profiles were visualized as a volcano plot and heat maps using the open source R language.

2.5. Functional enrichment analysis

Differential expression analyses were performed using the DESeq2 R package. Genes with an absolute fold change (FC) > 1.5 and a false discovery rate (FDR) < 0.05 were considered as differentially expressed genes (DEGs). The DEGs were then analyzed using Gene Ontology (GO) functional annotation and Kyoto Encyclopedia of Genes and Genomes (KEGG) pathway enrichment analysis with the DAVID 6.8 online analysis system (https://david.ncifcrf.gov/home.jsp). The genes with p-values < 0.05 after correction for FDR were considered as significant. Visualization was carried out using Cytoscape 3.6.0 software.

The entire gene expression profiles were applied to investigate the disease-related gene sets using gene set enrichment analysis (GSEA) software [28]. The list of the entire genome was ranked according to their expression values, and an enrichment score for each gene set was then calculated. The cumulative distribution function was constructed by performing 5000 random gene set membership assignments. The significance of the normalized enrichment score (NES) was determined by FDR < 25%.

2.6. Quantitative real-time PCR

Total RNA was extracted from the aorta of mice using Trizol Reagent (Invitrogen, 15596026), according to the manufacturer's protocol. Two micro grams of RNA was used to synthesize cDNA using the PrimeScript RT with gDNA Eraser reagent kit (Takara, RR047A). Quantitative real-time PCR was performed with TB Green Premix Ex Taq™ II (Takara, RR820A), gene-specific primers (250 nM final concentration of forward and reverse), and 2 μL cDNA. The relative expression level of the indicated genes was compared with that of a housekeeping gene β-actin, and expression fold changes were calculated using the $2^{-\triangle\triangle}$Ct method. The primer sequences used are listed in Table 1.

Table 1
Primer sequences for qRT-PCRs.

Gene	Forward Primer sequences (5'→3')	Reverse Primer sequences (5'→3')
αSMA/Acta2	GCCCAGAGCAAGAGAGG	TGTCAGCAGTGTCGGATG
SM22α/Tagln	TCCACAAACGACCAAGC	GGCCACACTGCACTACAA
Calponin1/Cnn1	ACCCCACGACATCTTTGA	CCGCTCTTGTTTCTCTGC
SMMHC/Myh11	TCCTCAATGCCTCCTCTG	GGTCCACATCCTTCCACA
β-Actin	TGGCATAGAGGTCTTTACGG	CAGCCTTCCTTCTTGGGTAT

2.7. Western blot analysis

Proteins were extracted from the aorta of mice and cultured cells, respectively. The total protein concentration was quantified using a BCA assay kit (Beyotime Institute of Biotechnology, P0012), according to the manufacturer's instructions. Protein samples were subjected to 10% SDS-PAGE and then transferred onto PVDF membranes (Millipore, USA). After blocking with 5% skimmed milk in Tris-buffered saline (TBS) and 0.1% Tween-20, the membranes were incubated with antibodies against αSMA (Proteintech, 14395-1-AP), SM22α (Abcam, ab14106), Calponin1 (CST, 17819), SMMHC (Proteintech, 21404-1-AP), and β-Actin (CST, 3700) overnight at 4 °C. The next day, membranes were washed, and incubated with appropriate peroxidase-conjugated secondary antibodies. The bands were visualized using an enhanced chemiluminescence system (ECL, Thermo). Blots were quantified by densitometric analysis using Image-Pro Plus software version 6.0.

2.8. Cell culture

The mouse aortic vascular smooth muscle cell line (MOVAS) was acquired from The American Type Culture Collection (ATCC, CRL-2797). Cells were cultured in Dulbecco's Modified Eagle Medium (DMEM) with high glucose (Gibco, 11965–092) supplemented with 10% fetal bovine serum (Biological Industries, 04-001-1ACS) at 37 °C in a 5% CO_2 humidified atmosphere. The cells were pre-stimulated in the presence or absence of ART (50 μM or 100 μM, purity ≥98%, Beijing Solarbio Life Sciences, IA0520) for 2 h followed by treatment with recombinant murine platelet-derived growth factor-BB (PDGF-BB, 20 ng/ml, PeproTech, 315–18) for 48 h [29]. Unless otherwise stated, cells were grown to sub-confluency (60%–70%) and then starved to synchronize for 2 h in DMEM containing 0.2% FBS before treatment. In all experiments, cells were subjected to no more than seven cell passages.

2.9. Wound healing assay

MOVAS cells were plated in six-well plates and cultured in complete medium for 24 h until 60% confluent. Then they were serum-starved for 2 h prior to further incubation in complete medium in the presence or absence of ART for a further 2 h before exposure to PDGF-BB. After a 48 h treatment, an identical wound was created across the center of the well with a sterile 200 μl pipette tip. The remaining cells were washed with PBS and cultured in DMEM. Three different areas of the wound gaps were photographed at a marked position at 0 and 48 h. The wound areas were measured by ImageJ software.

2.10. Transwell chamber assay

MOVAS cells were seeded in six-well plates and cultured in complete medium. After culturing for 24 h, the cells were serum-starved for 2 h prior to incubation in complete medium in the presence or absence of ART for a further 2 h before exposure to PDGF-BB. Then the cells (2×10^5 per well) were added to the upper chamber (8.0 μM pore size, Corning) in 200 μl of serum free DMEM. The lower chamber was filled with 600 μl DMEM containing 10% fetal bovine serum. After 24 h incubation, cells were fixed with 4% paraformaldehyde and stained with 0.1% crystal violet. Images of three different fields of each transwell membrane were acquired with a microscope.

2.11. Cell counting kit 8 (CCK8) assay

MOVAS cells were seeded into 96-well plates at a density of 2000 cells per well. After 24 h, the cells were serum-starved for 2 h, pretreated with ART for 2 h and then stimulated with PDGF-BB for 48 h. At 0, 24, 48, and 72 h after treatment, cell proliferation activity was detected using the CCK8 assay (MedChem Express, HY-P0093), according to the manufacturer's instructions. In brief, the media was replaced by fresh medium containing 10% CCK8 solution, and the plate was incubated at 37 °C for 1 h. The absorbance at 450 nm (A450) was examined using a scanning multi-well spectrophotometer (Bio-Tek, Synergy H1).

2.12. Statistical analysis

The results are presented as the mean ± standard error of the mean (SEM) of three or six independent experiments unless otherwise specified. One-way AVONA was used to assess the differences between more than two groups when the data conformed to a Gaussian distribution and homogeneity of variance. Tukey's multiple comparisons test was used for multiple comparisons between groups. If the data were not normally distributed, we carried out a Kruskal-Wallis test. Statistical significance was assumed when P-values were less than 0.05. All statistical analyses were calculated using the GraphPad Prism 8.0 (GraphPad Software Inc.).

3. Results

3.1. Artemisinin reduced atherosclerotic plaque development in ApoE−/− mice

Firstly, we examined the therapeutic effect of ART on $ApoE^{-/-}$ mice, which began to develop atherosclerotic plaques at six weeks of age and accelerated the formation of lesions by feeding them a Western diet [24]. The animal experimental grouping scheme is shown in Fig. 1a. The eight-week-old $ApoE^{-/-}$ mice were fed a Western diet and randomly allocated to receive ART (the chemical structure of artemisinin is shown in Fig. 1b) 50 mg/kg/day or 100 mg/kg/day by oral administration. To assess atherosclerotic lesions, we performed Oil Red O staining on the aortic roots (the plaque area measured at the aortic root and the entire aorta have a good correlation in an $ApoE^{-/-}$ mouse [30]). The results from the Oil Red O and HE stains demonstrated that the $ApoE^{-/-}$ mice treated with ART for eight weeks had a significantly smaller plaque area (Fig. 1c and d; 0.19 ± 0.02 mm^2, AS; 0.11 ± 0.01 mm^2, ART-L; 0.10 ± 0.01 mm^2, ART-H) and less cholesterol crystal deposit (Fig. 1e) when compared to the AS group. These results indicate that ART retarded the pathological plaque progression of atherosclerosis in $ApoE^{-/-}$ mice.

3.2. Overview of mRNA-Seq data and DEGs analysis

To understand the potential molecular mechanisms underlying the function of ART in the treatment of atherosclerosis, we performed

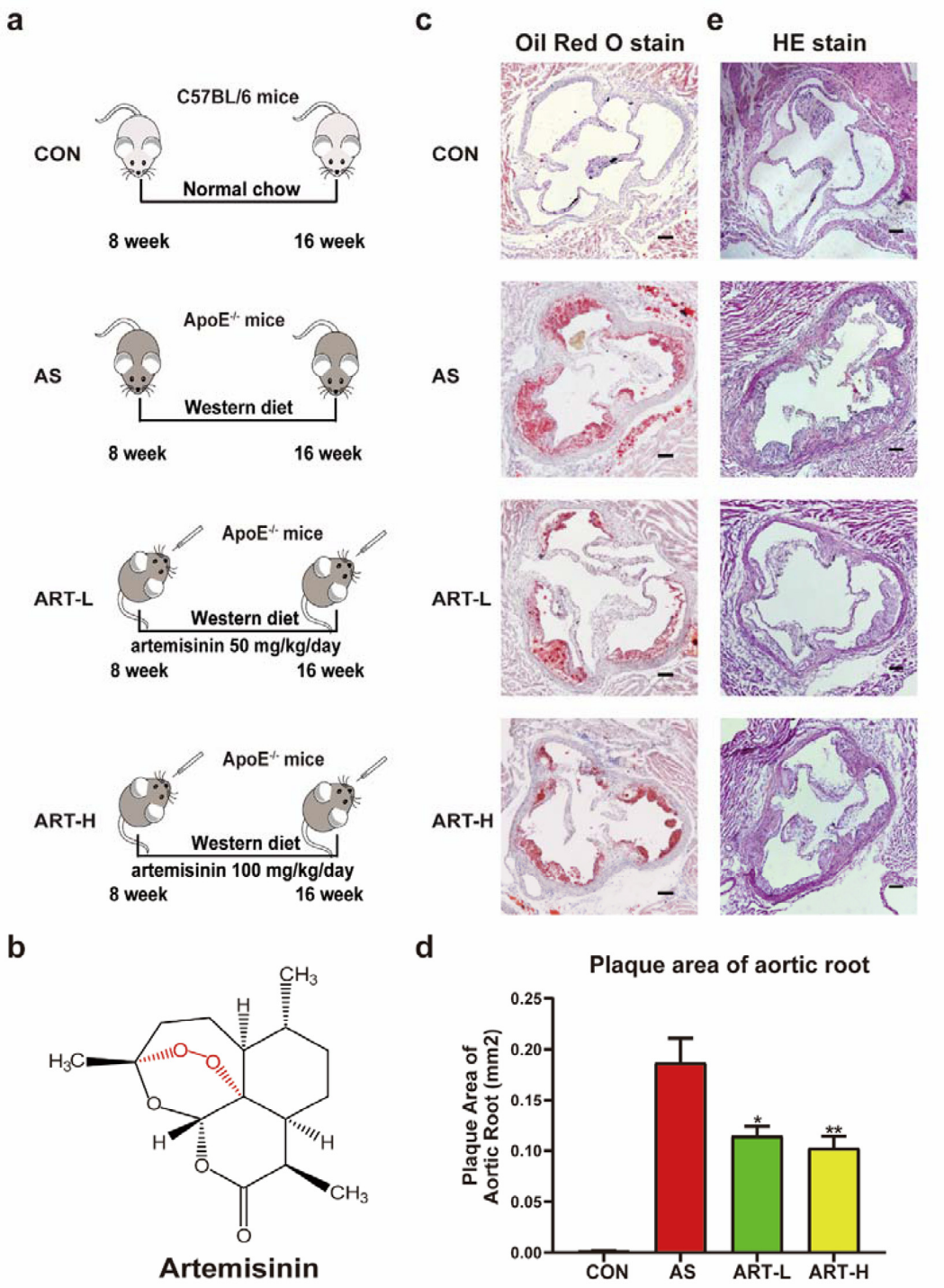

Fig. 1. Artemisinin reduced atherosclerotic plaque development in ApoE$^{-/-}$ mice. (a) Schematic illustration of the treatment and diet protocols. Eight weeks after birth, ApoE $^{-/-}$ mice were fed a Western diet and treated with ART for eight weeks. Sixteen-week-old mice were euthanized for tissue harvesting. (b) The chemical structure of artemisinin ($C_{15}H_{22}O_5$, Molecular Weight 282.33 g/mol, CAS number 63968-64-9) is a sesquiterpene lactone with an endoperoxide bridge (marked in red). (c) Aortic root sections stained with Oil Red O (Scale bar = 100 μM). (d) Quantification of the plaque areas (mm^2) from Oil Red O-stained sections of aortic root. *P < 0.05, **P < 0.01 in compared with the AS group (e) Representative images of aortic root sections were stained with H&E (Scale bar = 100 μM). All experiments presented as mean ± SEM of n = 6 biologically independent sample. One-way ANOVA calculation of P-values with Tukey's multiple comparisons test. . (For interpretation of the references to color in this figure legend, the reader is referred to the Web version of this article.)

whole transcriptome sequencing of aortas (three from mice in the AS group and three from mice in the ART-L group). To avoid bias caused by the expression of low abundance gene, we removed the sequences with read counts below ten per sample, before analysis. We identified 220 genes which were up-regulated, and 457 genes, which were down-regulated after ART treatment. The DESeq2 R package was used to calculate the differentially expressed genes (DEGs) with a threshold for a false discovery rate (FDR) of < 0.05 and absolute fold change of > 1.5. The genes were visualized using a volcano plot (Fig. 2a). Next we used an unsupervised hierarchical cluster heat map to demonstrate the patterns of gene expression between the ART-L and AS groups. As shown in Fig. 2b, we could detect a distinct change in gene expression

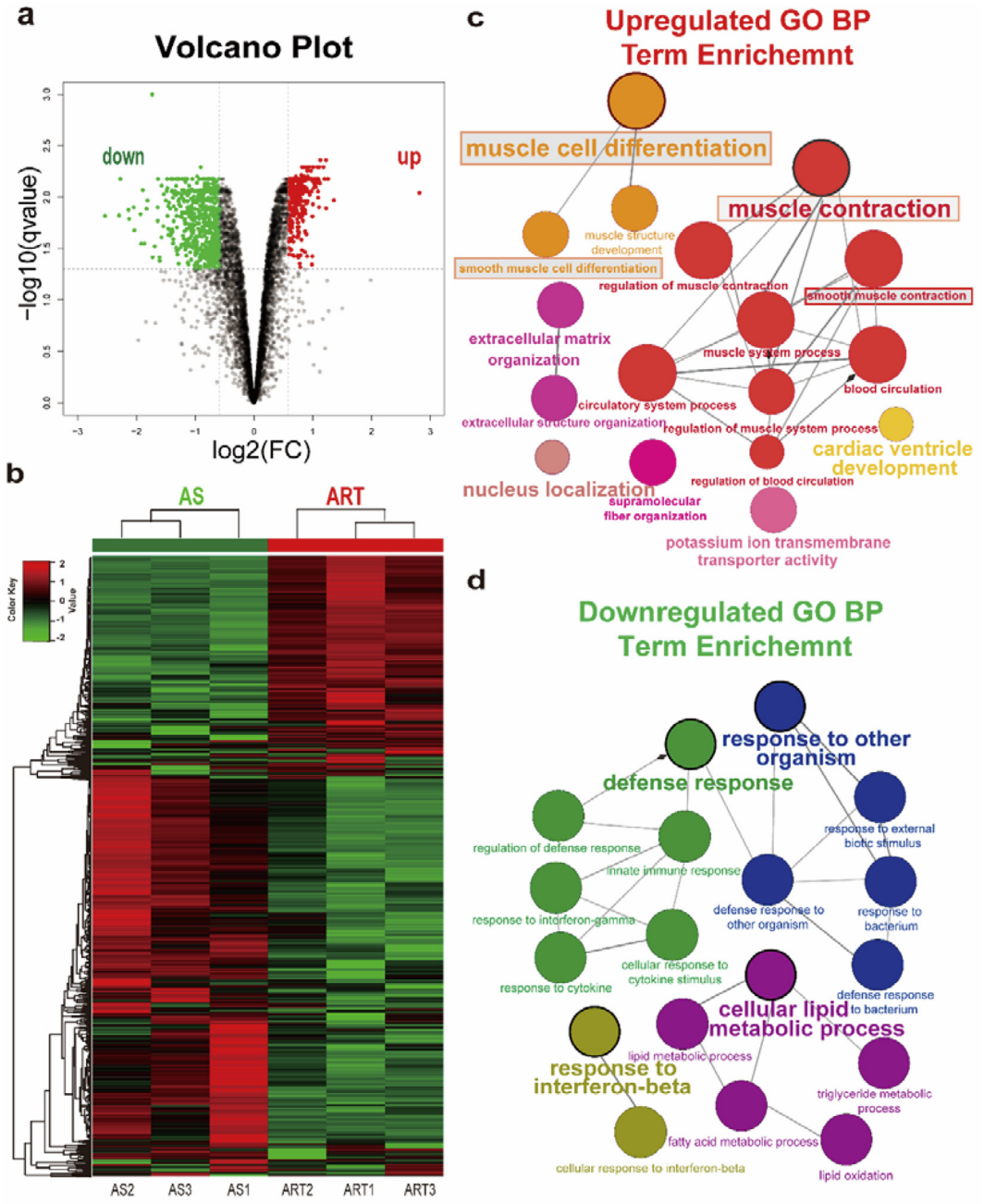

Fig. 2. mRNA expression patterns in the ART-L and AS groups and GO analysis of upregulated differentially expressed genes. (a) Volcano plot demonstrating global gene expression changes following mRNA sequencing analysis on aortas from mice in the AS and ART-L groups. The red and green dots on the graph represent up-regulated and down-regulated mRNA in the ART-L group, respectively. The vertical dotted lines correspond to a 1.5-fold change (FC) up and down, and the horizontal dotted line represents an FDR of 0.05. (b) Hierarchical cluster heatmap of differential mRNA expression patterns. Red and green signals indicate up and down-regulated expression after ART treatment. (c) and (d) The clustered network of significantly over-represented gene ontology (GO) terms in a biological process. The node size is based on -log10 (adjust p-value) and its color is dependent upon the Kappa score. Bonferroni correction was applied to the p-value. . (For interpretation of the references to color in this figure legend, the reader is referred to the Web version of this article.)

patterns after the mice treated with ART. These gene expression changes may give clues as to the pharmacological mechanism of action of ART as an anti-atherosclerosis agent. Therefore, the DEGs were selected to performed functional annotation enrichment analysis. We used the online analysis system DAVID 6.8 to carry out functional annotation of the up-regulated and down-regulated DEGs in the ART-L group [31], and the significantly enriched gene ontology (GO) terms of biological processes were displayed as a clustered network by ClueGO software [32] (Fig. 2c and d). Interestingly, the top three most significantly upregulated GO terms were muscle contraction (GO:0006936), muscle cell differentiation (GO:0042692) and smooth muscle contraction (GO:0006939), which correlate with a vascular smooth muscle contractile phenotype (differentiated phenotype). Other statistically significant enriched GO terms are detailed in Table 2. The top three most significantly downregulated GO terms were response to other organism (GO:0051707), response to external biotic stimulus (GO:0043207), and response to biotic stimulus (GO:0009607). Overall, these results indicated that ART treatment induced aortic gene expression profile changes in ApoE$^{-/-}$ and that these altered genes were mainly enriched for the terms involving (smooth) muscle cell differentiation processes.

Table 2
Go BP Term significantly up-regulated in the artemisinin group.

GO ID	GO Term	Term P-Value Corrected	% Associated Genes	Nr. Genes
GO:0006936	muscle contraction	1.19548E-06	10.34	15
GO:0042692	muscle cell differentiation	8.11722E-06	6.60	20
GO:0006939	smooth muscle contraction	2.27348E-05	16.67	9
GO:0003012	muscle system process	3.91523E-05	7.44	16
GO:0008015	blood circulation	4.77327E-05	6.52	18
GO:0003013	circulatory system process	8.47082E-05	6.27	18
GO:0006937	regulation of muscle contraction	0.000194105	13.04	9
GO:0061061	muscle structure development	0.000599091	4.40	24
GO:0097435	supramolecular fiber organization	0.001152096	5.47	17
GO:0051145	smooth muscle cell differentiation	0.001460139	14.58	7
GO:0030198	extracellular matrix organization	0.00182895	6.67	13
GO:0090257	regulation of muscle system process	0.002505784	8.47	10
GO:0015079	potassium ion transmembrane transporter activity	0.003130223	10.81	8
GO:0043062	extracellular structure organization	0.00438712	6.13	13
GO:0051647	nucleus localization	0.00728944	19.23	5
GO:1903522	regulation of blood circulation	0.007355951	7.46	10
GO:0003231	cardiac ventricle development	0.009994058	7.19	10

3.3. KEGG and GSEA pathway enrichment analysis of the aorta by mRNA-Seq

To further gain an insight into the key pathways involved in the anti-atherosclerosis effect of ART, we used two different tools to perform our bioinformatics analysis. KEGG [33] is an over-representation analysis (ORA), and was used to enrich the functional pathways seen in up and down-regulated DEGs. The results are shown in the bubble charts below (Fig. 3a and b). Interestingly, the vascular smooth muscle contraction item was the most significantly enriched pathway in the ART treatment group. We also used GSEA, which is based on functional class scoring (FCS), and was employed to analyze disease-related phenotypes, which is a method considered the expression values of all genes. The two datasets with the highest normalized enrichment score were the smooth muscle contraction dataset (NES = 1.92, FDR = 0.049) and the unstable atherosclerotic plaque down dataset (NES = 2.03, FDR = 0.014), and both have a positive correlation with the ART treatment group (Fig. 3c and d). In summary, both KEGG and GSEA pathway enrichment analysis showed that the vascular smooth muscle contraction functional set was the most significantly changed pathway following administration of ART to mice.

3.4. Artemisinin treatment increases VSMC contractile phenotypic markers in the aortas of mice

Enrichment analysis demonstrated that the most prominent effects of ART on the aorta of mice were changes in the gene expressions of vascular smooth muscle contraction pathways when compared to the non-treated controls. Firstly, we validated the mRNA levels of the relevant genes in the aorta of mice by qRT-PCR (Fig. 4b). Consistent with current reports of VSMC transition from a contractile phenotype to a de-differentiated synthetic phenotype during atherosclerosis, we found the expression of the contractile phenotype genes αSMA, SM22α, calponin1, and SMMHC were decreased in the aorta of the AS group when compared to the control group. These genes were expressed higher in the ART treatment group when compared to the AS group. This is in accordance with the expression values from the RNA sequencing data (demonstrated by a heatmap, Fig. 4a). Next we further explored the protein expression levels of these genes using western blot (Fig. 4c). As expected, we found that αSMA, SM22α, calponin1, and SMMHC protein levels increased significantly after ART treatment (Fig. 4d). In line with our previous enrichment analysis results, both qRT-PCR and western blot analyses demonstrated that the expression of the VSMC contractile phenotype markers was raised in the aorta of $ApoE^{-/-}$ mice after treated with ART.

3.5. Artemisinin suppressed PDGF-induced VSMC migration, proliferation and de-differentiation

To further verify our *in vivo* findings, we selected MOVAS cells to establish a VSMC phenotype switching model *in vitro*. PDGF-BB is the most widely reported cytokine to induce VSMC migration, proliferation and phenotypic switching from a contractile phenotype to a pathological synthetic phenotype [12]. Therefore, we applied PDGF-BB (20 ng/ml) to stimulate MOVAS cells, which had been pre-treated with ART (50 μM or 100 μM; for 2 h). We first examined the proliferation and migration capacity of the cells using a wound healing experiment, a transwell assay and a CCK8 assay, respectively. In this study, we observed that PDGF-BB treatment visibly promoted the migration and proliferation of MOVAS cells. However, ART can effectively reverse the PDGF-promoted cell migration and proliferation (Fig. 5a–e). We next detected contractile phenotype marker expression levels using western blot, and Fig. 5f shows the results of one representative experiment. Western blotting revealed that PDGF-BB treatment decreased the expressions of αSMA, SM22α, calponin1 and SMMHC. However, as observed *in vivo*, an increase in expression of these contractile phenotype marker was noted in the ART treatment group (Fig. 5g). Taken together, these results indicate that ART attenuated MOVAS cell migration and proliferation and elevates the expression of contractile phenotype proteins under PDGF-stimulated conditions.

4. Discussion

The present study demonstrates a novel pharmacological effect of ART involving the attenuation of atherosclerosis progression. This effect at least in part is through the inhibition of VSMC phenotype switching from a contractile to de-differentiated phenotype. Our findings indicate that ART plays a protective role in atherosclerosis and can reduce atherosclerotic plaque size in $ApoE^{-/-}$ mice. As high-throughput sequencing experiments in mouse models of atherosclerosis treated with ART have not yet been reported previously, we performed RNA sequencing of aortas to provide a global insight into the underlying pharmacological mechanism of the anti-atherosclerotic effect of ART. Bioinformatic analysis of the sequencing data using three different algorithms showed that the vascular smooth muscle contractile functional set was the most significantly enriched pathway. Consistent with the results of RNA-seq analysis, ART could significantly increase the expression of contractile phenotype markers in the aorta of $ApoE^{-/-}$ mice and effectively reverse PDGF-promote MOVAS cell migration, proliferation, and de-differentiation. These results imply that ART is an excellent candidate for the treatment of atherosclerosis.

Atherosclerosis is a slowly progressing disease during which many

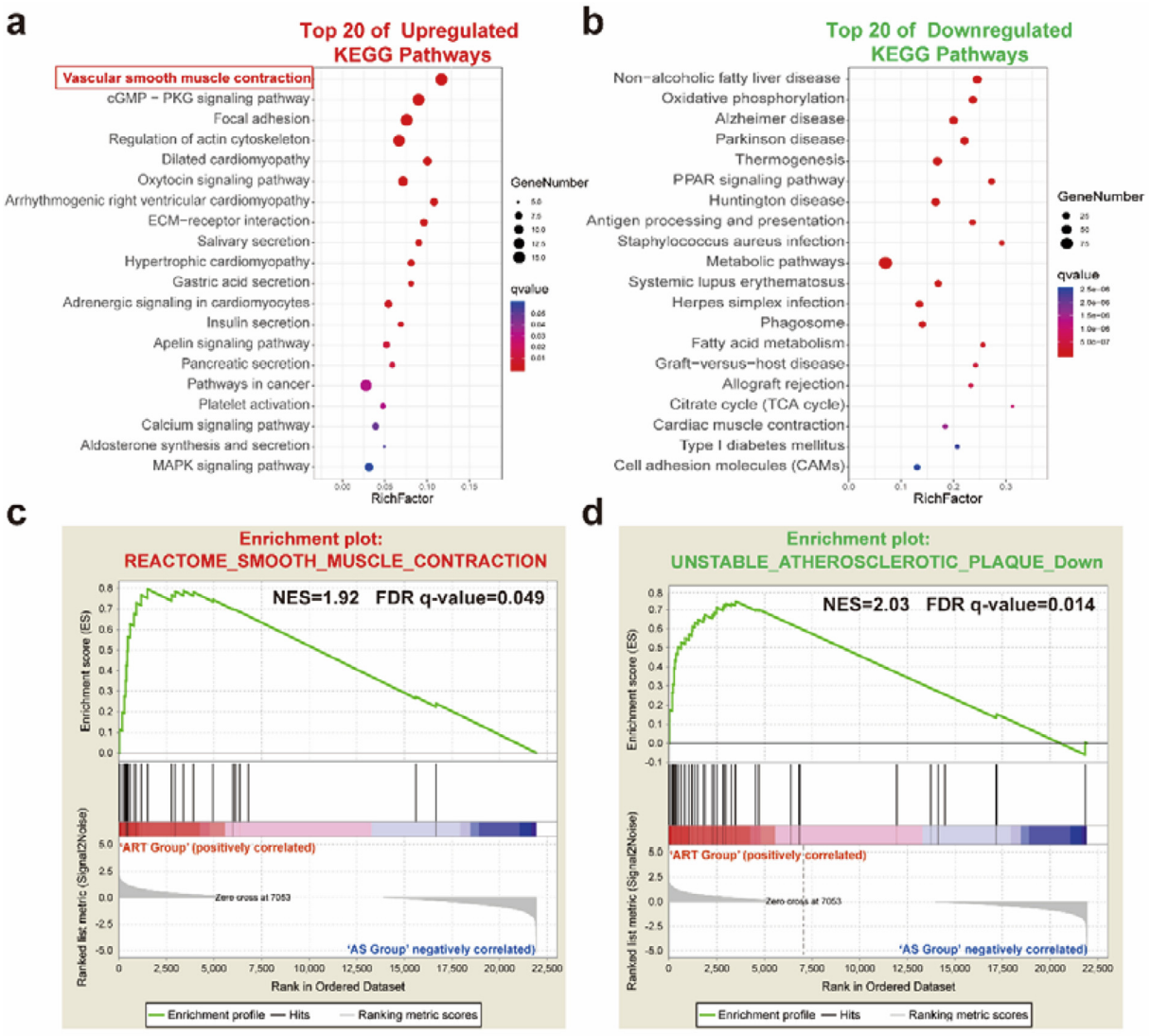

Fig. 3. KEGG pathway enrichment analysis and gene set enrichment analysis (GSEA). (a) and (b) Bubble chart shows the top 20 significantly enriched KEGG pathways from the up and down-regulated DEGs in the ART-L group, according to the P-value. The X-axis represents the enrichment factor (the ratio between the number of differentially expressed genes and all uniGenes enriched in a particular pathway). The Y-axis corresponds to KEGG pathways. (c) and (d) Gene set enrichment analysis (GSEA) shows the positively enriched disease-related gene sets. The horizontal bar in graded color from red to blue represents the rank-ordered, non-redundant list of genes. The vertical black lines represent the projection of individual genes onto the ranked gene list. Genes on the left side (red) indicate the gene set enriched in the ART-L group. Permutation = 5000; NES, normalized enrichment score; FDR, false discovery rate. . (For interpretation of the references to color in this figure legend, the reader is referred to the Web version of this article.)

cell types become dysfunctional. For example the abnormal activation of endothelial cells, phenotypic switching of VSMCs, and pro-inflammatory differentiation of leukocytes. Previous studies looking at the progression of atherosclerosis has mainly focused on endothelial cells and leukocytes. However, recently the combination of two emerging genetic engineering technologies, lineage-tracing and single-cell sequencing, has given a tremendous ability for researchers to follow the transitions of different cell types during their development and progression during atherosclerosis. Using these methods there is no need to identify the cells by their 'specific' markers (the cells may de-differentiate and lose their original functional markers or gain other cell type specific markers). Surprisingly, lineage-tracing research has unambiguously revealed that VSMCs contribute substantially to the formation of atherosclerotic plaques, generating forty to seventy percent of all plaque cells [4–6]. Moreover, combining single-cell sequencing with VSMC lineage tracing demonstrated a pronounced heterogeneity of VSMCs in the aortas of atherosclerotic mouse models [7–9]. This implies that VSMCs undergo de-differentiation and display multiple transcriptional expression profiles. These novel findings highlighted an important role for VSMCs during atherosclerosis progression and has attracted a greater number of investigations into VSMC phenotype switching. As a result, identifying drugs that inhibit VSMC phenotype switching to the de-differentiated phenotype may be a therapeutic strategy against atherosclerosis.

ART is currently the most effective anti-malarial drug. It is from a family of sesquiterpene lactones containing a unique chemical structure (endoperoxide bridge) which is believed to be responsible for its pharmacological mechanism of antimalarial activity [34]. However, in recent years, publications relating to ART in non-malarial research have steadily grown. With its safety record for treating millions of people infected with malaria, ART has been investigated in cancers, autoimmune diseases, allergic disorders, and many other diseases. During the past decade, ART has been reported to demonstrate a strong inhibitory effect against various cancer types by causing cell cycle arrest,

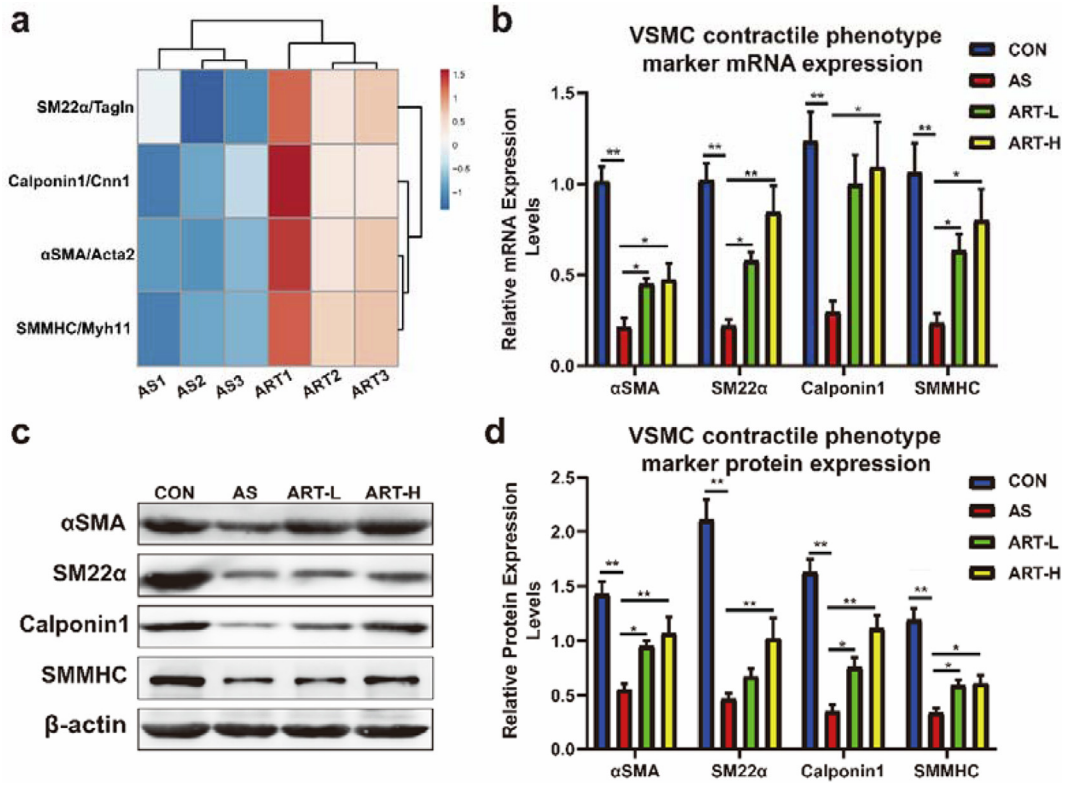

Fig. 4. Artemisinin treatment increased VSMC contractile phenotype markers in the aorta of mice. (a) A heatmap representing the expressions of VSMC contractile phenotype related genes in the RNA-sequencing data. (b) The expression of VSMC contractile phenotype related gene in the aorta of mice was determined by qRT-PCR. The relative expression levels of the indicated genes were normalized to the values of the control group, and β-actin was used as the endogenous control. (c) The contractile phenotype proteins αSMA, SM22α, calponin1, and SMMHC are shown by western blot, (d) and the relative expression was normalized to β-actin. The results are shown as mean ± SEM from six independent experiments. One-way ANOVA calculated the P values with Tukey's multiple comparisons test. Asterisks indicate significances: *P < 0.05 and **P < 0.01.

inducing apoptosis, inhibiting angiogenesis, and eliminating tumor invasion and metastasis. Furthermore, with compelling evidence from many researchers on the effect of ART as an anti-tumor treatment, studies on the pharmacological effects of ART have entered phase I/II clinical trials in lung carcinoma [35], breast carcinoma [36], colorectal carcinoma [37].

Recently, some researchers have reported that ART can attenuate inflammatory symptoms in experimental rheumatoid arthritis by suppressing pro-inflammatory cytokines, such as TNF-α, IL-1β, IL-6, IL-8 and inhibiting mitogen activated protein kinase (MAPK) and NF-κB signaling pathways [38,39]. These anti-inflammatory effects attracted considerable attention, and currently artemisinin is being investigated for the treatment of other inflammatory diseases, such as inflammatory bowel disease [40], neuroinflammation [41], and nephritis [42]. However, very little is known about the role of artemisinin in atherosclerosis. Therefore, we selected eight-week-old male ApoE−/− mice to treat with ART for eight weeks to explore its effect. Our data showed a smaller plaque area in ApoE$^{-/-}$ mice after ART treatment. This result is in line with Jiang's findings where artesunate, a derivative of ART, could attenuate atherosclerotic progression in aortas of ApoE$^{-/-}$ mice when treated for six months [43].

Modern high-throughput sequencing technology creates opportunities for analysis of global gene expression patterns. To gain an insight into the key pathways involved in the anti-atherosclerosis effect of ART, we performed functional enrichment analysis of our RNA-Seq data. Our data showed the top 20 significantly enriched pathways that were up- or down-regulated, and the vascular smooth muscle contraction functional set was deemed the most important pathway produced by ART treatment. Next, we conducted *in vivo* and *in vitro* experiments for verification. In accordance with the results of enrichment analysis, ART could significantly increase the expression of contractile phenotype markers in the aorta of ApoE$^{-/-}$ mice and effectively reverse PDGF-promoted MOVAS cell migration, proliferation, and de-differentiation. The findings of Jiang showed that artesunate could attenuate atherosclerotic progression and down-regulate pro-inflammatory cytokines (TNF-α, IL-6, IL-8, and MCP-1) [43], and the other enriched pathways mentioned above from our RNA-Seq data. This suggests that ART might also exert its anti-atherosclerosis effect by the use of multiple pathways, and this deserves further investigation.

In summary, our results have demonstrated a previously unknown function for ART involving the suppression of atherosclerosis progression, at least in part through inhibition of VSMC phenotype switching from a contractile to a de-differentiated phenotype. These observations have opened up novel therapeutic possibilities for atherosclerosis treatment.

5. Conclusion

The findings from this study demonstrate a pharmacological action of ART as an anti-atherosclerosis treatment. Artemisinin attenuated the progression of atherosclerosis partly through the inhibition of VSMC phenotypic switching from a contractile to a de-differentiated phenotype. Our data indicated that ART is a promising candidate for the potential treatment of atherosclerosis.

Author contributions

Design and conduct of the study: Hongjiao Du, Qiao Zhao, Xiaodong Li.

Data collection and analysis: Hongjiao Du, Hongbin Zang.

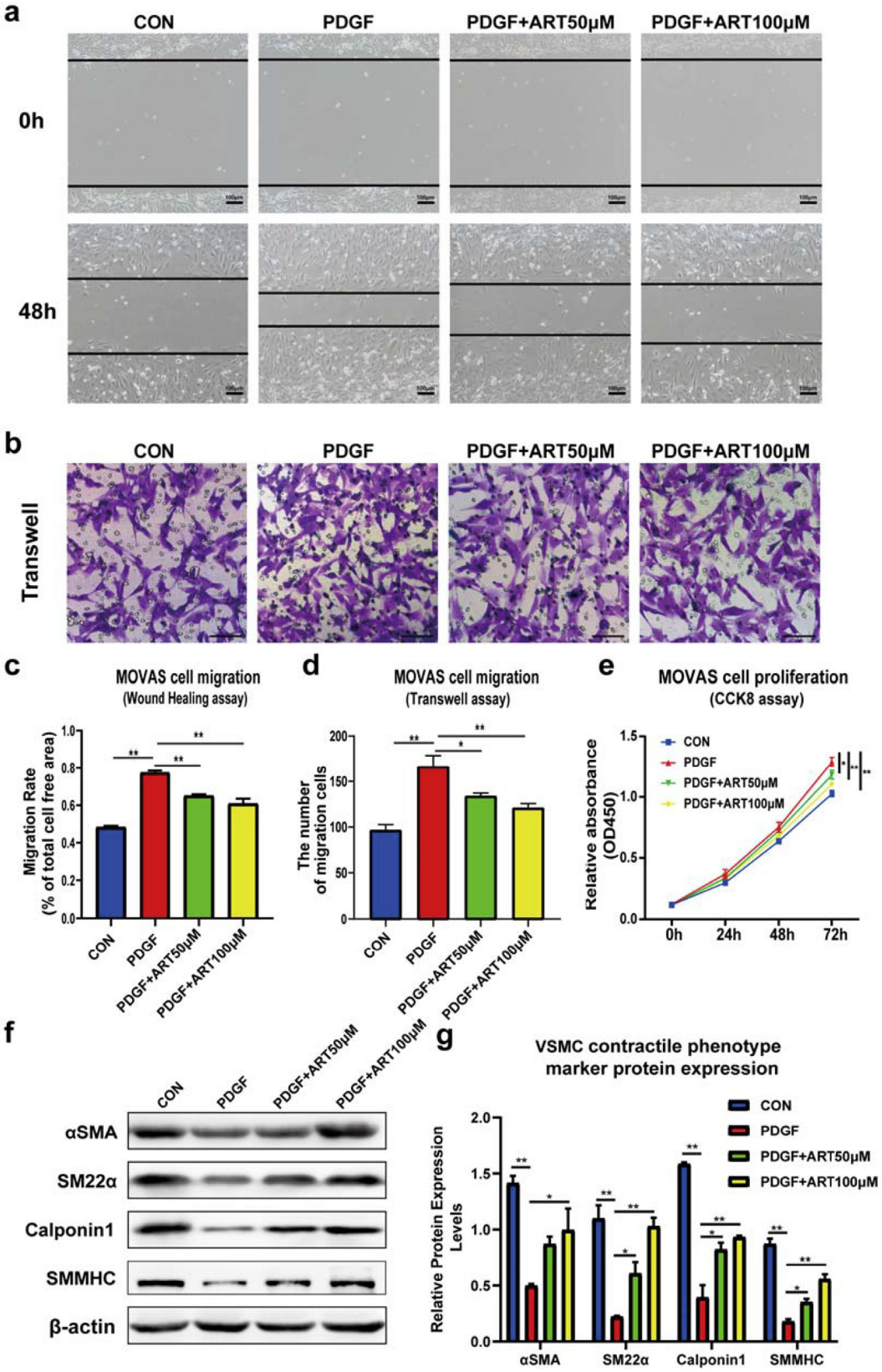

Fig. 5. Artemisinin suppressed PDGF-induced VSMC migration, proliferation and de-differentiation. (a) Wound healing assays were performed, and pictures were taken at 0 and 48 h time points. (b) The migration capacity of the cells was determined by transwell assay (Scale bar = 100 μM). (c) Quantitative analysis of migration distance. The cell migration area as a percentage of the total cell-free area was calculated. (d) Quantitative analysis of the number of migration cells. (e) Cell proliferation was measured using the CCK8 assay kit. The number of cells was quantified in units of optical density (OD450). (f) Cultured MOVAS cells expressed contractile phenotype proteins such as αSMA, SM22α, calponin1 and SMMHC as shown by western blotting (g) and their relative expression was normalized to β-actin. The results are shown as mean ± SEM from three independent experiments. One-way ANOVA calculated the P values with Tukey's multiple comparisons test. Asterisks indicate significance: *P < 0.05 and **P < 0.01. MOVAS indicates mouse aortic vascular smooth muscle cell line.

Data interpretation: Hongjiao Du, Hongbin Zang, Cheng Chang.

Manuscript writing: Hongjiao Du, Qiao Zhao, Hongbin Zang, Cheng Chang, Xiaodong Li.

All authors have read and approved the final version of the article.

Declaration of competing interest

All authors declare no conflict of interest.

Acknowledgements

This work was supported by a grant from the Key Science and Technology Project of Liaoning Province (No. 2017225007).

References

[1] E.J. Benjamin, S.S. Virani, C.W. Callaway, A.M. Chamberlain, A.R. Chang, S. Cheng, et al., Heart disease and stroke statistics-2018 update: a report from the American heart association, Circulation 137 (2018) e67–e492.

[2] S.J. Nicholls, R. Puri, T. Anderson, C.M. Ballantyne, L. Cho, J.J. Kastelein, et al., Effect of evolocumab on progression of coronary disease in statin-treated patients: the GLAGOV randomized clinical trial, J. Am. Med. Assoc. 316 (2016) 2373–2384.

[3] P. Libby, K.E. Bornfeldt, A.R. Tall, Atherosclerosis: successes, surprises, and future challenges, Circ. Res. 118 (2016) 531–534.

[4] J. Albarran-Juarez, H. Kaur, M. Grimm, S. Offermanns, N. Wettschureck, Lineage tracing of cells involved in atherosclerosis, Atherosclerosis 251 (2016) 445–453.

[5] K. Jacobsen, M.B. Lund, J. Shim, S. Gunnersen, E.M. Fuchtbauer, M. Kjolby, et al., Diverse cellular architecture of atherosclerotic plaque derives from clonal expansion of a few medial SMCs, JCI Insight 2 (2017).

[6] J. Chappell, J.L. Harman, V.M. Narasimhan, H. Yu, K. Foote, B.D. Simons, et al., Extensive proliferation of a subset of differentiated, yet plastic, medial vascular smooth muscle cells contributes to neointimal formation in mouse injury and atherosclerosis models, Circ. Res. 119 (2016) 1313–1323.

[7] K. Van Kuijk, C. Kuppe, C. Betsholtz, M. Vanlandewijck, R. Kramann, J.C. Sluimer, Heterogeneity and plasticity in healthy and atherosclerotic vasculature explored by single cell sequencing, Cardiovasc. Res. 115 (2019) 1705–1715.

[8] L. Dobnikar, A.L. Taylor, J. Chappell, P. Oldach, J.L. Harman, E. Oerton, et al., Disease-relevant transcriptional signatures identified in individual smooth muscle cells from healthy mouse vessels, Nat. Commun. 9 (2018) 4567.

[9] H. Kaur, J. Carvalho, M. Looso, P. Singh, R. Chennupati, J. Preussner, et al., Single-cell profiling reveals heterogeneity and functional patterning of GPCR expression in the vascular system, Nat. Commun. 8 (2017) 15700.

[10] G.K. Owens, Regulation of differentiation of vascular smooth muscle cells, Physiol. Rev. 75 (1995) 487–517.

[11] S. Allahverdian, C. Chaabane, K. Boukais, G.A. Francis, M.L. Bochaton-Piallat, Smooth muscle cell fate and plasticity in atherosclerosis, Cardiovasc. Res. 114 (2018) 540–550.

[12] G.L. Basatemur, H.F. Jorgensen, M.C.H. Clarke, M.R. Bennett, Z. Mallat, Vascular smooth muscle cells in atherosclerosis, Nat. Rev. Cardiol. (2019).

[13] D. Gomez, G.K. Owens, Smooth muscle cell phenotypic switching in atherosclerosis, Cardiovasc. Res. 95 (2012) 156–164.

[14] L.S. Shankman, D. Gomez, O.A. Cherepanova, M. Salmon, G.F. Alencar, R.M. Haskins, et al., KLF4-dependent phenotypic modulation of smooth muscle cells has a key role in atherosclerotic plaque pathogenesis, Nat. Med. 21 (2015) 628–637.

[15] O.A. Cherepanova, D. Gomez, L.S. Shankman, P. Swiatlowska, J. Williams, O.F. Sarmento, et al., Activation of the pluripotency factor OCT4 in smooth muscle cells is atheroprotective, Nat. Med. 22 (2016) 657–665.

[16] R.C. Wirka, D. Wagh, D.T. Paik, M. Pjanic, T. Nguyen, C.L. Miller, et al., Atheroprotective roles of smooth muscle cell phenotypic modulation and the TCF21 disease gene as revealed by single-cell analysis, Nat. Med. 25 (2019) 1280–1289.

[17] D.L. Klayman, Qinghaosu (artemisinin): an antimalarial drug from China, Science 228 (1985) 1049–1055.

[18] B.J. Visser, R.W. Wieten, D. Kroon, I.M. Nagel, S. Belard, M. van Vugt, et al., Efficacy and safety of artemisinin combination therapy (ACT) for non-falciparum malaria: a systematic review, Malar. J. 13 (2014) 463.

[19] S. Zhu, W. Liu, X. Ke, J. Li, R. Hu, H. Cui, et al., Artemisinin reduces cell proliferation and induces apoptosis in neuroblastoma, Oncol. Rep. 32 (2014) 1094–1100.

[20] W.D. Li, Y.J. Dong, Y.Y. Tu, Z.B. Lin, Dihydroarteannuin ameliorates lupus symptom of BXSB mice by inhibiting production of TNF-alpha and blocking the signaling pathway NF-kappa B translocation, Int. Immunopharmacol. 6 (2006) 1243–1250.

[21] T. Efferth, M.R. Romero, D.G. Wolf, T. Stamminger, J.J. Marin, M. Marschall, The antiviral activities of artemisinin and artesunate, Clin. Infect. Dis. 47 (2008) 804–811.

[22] P. Lu, F.C. Zhang, S.W. Qian, X. Li, Z.M. Cui, Y.J. Dang, et al., Artemisinin derivatives prevent obesity by inducing browning of WAT and enhancing BAT function, Cell Res. 26 (2016) 1169–1172.

[23] B. Zhang, P. Liu, Y. Zhou, Z. Chen, Y. He, M. Mo, et al., Dihydroartemisinin attenuates renal fibrosis through regulation of fibroblast proliferation and differentiation, Life Sci. 223 (2019) 29–37.

[24] B. Emini Veseli, P. Perrotta, G.R.A. De Meyer, L. Roth, C. Van der Donckt, W. Martinet, et al., Animal models of atherosclerosis, Eur. J. Pharmacol. 816 (2017) 3–13.

[25] B. Paigen, A. Morrow, P.A. Holmes, D. Mitchell, R.A. Williams, Quantitative assessment of atherosclerotic lesions in mice, Atherosclerosis 68 (1987) 231–240.

[26] M. Pertea, D. Kim, G.M. Pertea, J.T. Leek, S.L. Salzberg, Transcript-level expression analysis of RNA-seq experiments with HISAT, StringTie and Ballgown, Nat. Protoc. 11 (2016) 1650–1667.

[27] C. Trapnell, B.A. Williams, G. Pertea, A. Mortazavi, G. Kwan, M.J. van Baren, et al., Transcript assembly and quantification by RNA-Seq reveals unannotated transcripts and isoform switching during cell differentiation, Nat. Biotechnol. 28 (2010) 511–515.

[28] A. Subramanian, P. Tamayo, V.K. Mootha, S. Mukherjee, B.L. Ebert, M.A. Gillette, et al., Gene set enrichment analysis: a knowledge-based approach for interpreting genome-wide expression profiles, Proc. Natl. Acad. Sci. U. S. A. 102 (2005) 15545–15550.

[29] B.J. Holycross, R.S. Blank, M.M. Thompson, M.J. Peach, G.K. Owens, Platelet-derived growth factor-BB-induced suppression of smooth muscle cell differentiation, Circ. Res. 71 (1992) 1525–1532.

[30] R.K. Tangirala, E.M. Rubin, W. Palinski, Quantitation of atherosclerosis in murine models: correlation between lesions in the aortic origin and in the entire aorta, and differences in the extent of lesions between sexes in LDL receptor-deficient and apolipoprotein E-deficient mice, J. Lipid Res. 36 (1995) 2320–2328.

[31] da W. Huang, B.T. Sherman, R.A. Lempicki, Bioinformatics enrichment tools: paths toward the comprehensive functional analysis of large gene lists, Nucleic Acids Res. 37 (2009) 1–13.

[32] G. Bindea, B. Mlecnik, H. Hackl, P. Charoentong, M. Tosolini, A. Kirilovsky, et al., ClueGO: a Cytoscape plug-in to decipher functionally grouped gene ontology and pathway annotation networks, Bioinformatics 25 (2009) 1091–1093.

[33] M. Kanehisa, M. Furumichi, M. Tanabe, Y. Sato, K. Morishima, KEGG: new perspectives on genomes, pathways, diseases and drugs, Nucleic Acids Res. 45 (2017) D353–D361.

[34] J. Wang, C.J. Zhang, W.N. Chia, C.C. Loh, Z. Li, Y.M. Lee, et al., Haem-activated promiscuous targeting of artemisinin in Plasmodium falciparum, Nat. Commun. 6 (2015) 10111.

[35] T. Efferth, From ancient herb to modern drug: Artemisia annua and artemisinin for cancer therapy, Semin. Cancer Biol. 46 (2017) 65–83.

[36] C. von Hagens, I. Walter-Sack, M. Goeckenjan, J. Osburg, B. Storch-Hagenlocher, S. Sertel, et al., Prospective open uncontrolled phase I study to define a well-tolerated dose of oral artesunate as add-on therapy in patients with metastatic breast cancer (ARTIC M33/2), Breast Canc. Res. Treat. 164 (2017) 359–369.

[37] S. Krishna, S. Ganapathi, I.C. Ster, M.E. Saeed, M. Cowan, C. Finlayson, et al., A randomised, double blind, placebo-controlled pilot study of oral artesunate therapy for colorectal cancer, EBioMedicine 2 (2015) 82–90.

[38] M. Fan, Y. Li, C. Yao, X. Liu, X. Liu, J. Liu, Dihydroartemisinin derivative DC32 attenuates collagen-induced arthritis in mice by restoring the Treg/Th17 balance and inhibiting synovitis through down-regulation of IL-6, Int. Immunopharmacol. 65 (2018) 233–243.

[39] Y. Li, S. Wang, Y. Wang, C. Zhou, G. Chen, W. Shen, et al., Inhibitory effect of the antimalarial agent artesunate on collagen-induced arthritis in rats through nuclear factor kappa B and mitogen-activated protein kinase signaling pathway, Transl. Res. 161 (2013) 89–98.

[40] Y.X. Yan, M.J. Shao, Q. Qi, Y.S. Xu, X.Q. Yang, F.H. Zhu, et al., Artemisinin analogue SM934 ameliorates DSS-induced mouse ulcerative colitis via suppressing neutrophils and macrophages, Acta Pharmacol. Sin. 39 (2018) 1633–1644.

[41] Z. Shi, Y. Chen, C. Lu, L.M. Dong, J.W. Lv, Q.H. Tuo, et al., Resolving neuroinflammation, the therapeutic potential of the anti-malaria drug family of artemisinin, Pharmacol. Res. 136 (2018) 172–180.

[42] Z. Sun, Y. Ma, F. Chen, S. Wang, B. Chen, J. Shi, Artesunate ameliorates high glucose-induced rat glomerular mesangial cell injury by suppressing the TLR4/NF-kappaB/NLRP3 inflammasome pathway, Chem. Biol. Interact. 293 (2018) 11–19.

[43] W. Jiang, Y. Cen, Y. Song, P. Li, R. Qin, C. Liu, et al., Artesunate attenuated progression of atherosclerosis lesion formation alone or combined with rosuvastatin through inhibition of pro-inflammatory cytokines and pro-inflammatory chemokines, Phytomedicine 23 (2016) 1259–1266.